On the Performance of Practical Pulse-Shaped OTFS with Analog Receivers

Andong Zhou*, Yanjun Pan,† *Member, IEEE*, Jingxian Wu,* *Senior Member, IEEE*, Hai Lin,‡ *Senior Member, IEEE*, and Jinhong Yuan,⋆ *Fellow, IEEE*

***Abstract*—We study the impacts of practical pulse-shaping on the performance of orthogonal time frequency space (OTFS) systems with a matched filter based analog receiver. Unlike most existing OTFS works that use a sampling and DFT-based digital receiver, we investigate the OTFS waveform in a precise manner by strictly following the continuous-time Heisenberg and Wigner transforms as in the original OTFS architecture. Closed-form expressions of the cross-ambiguity functions of several practical pulses are developed to facilitate the modeling and analysis of the analog architecture. In particular, we derive a matrix representation of the input-output relationship of the OTFS system with the help of an equivalent discrete delay-Doppler channel spread function, which incorporates the combined effects of the physical propagation channel, the bandwidth and duration restrictions imposed on the OTFS signals, and the transmit and receive pulses. Numerical results demonstrated that *under the analog OTFS architecture*, practical rectangular pulse-shaping waveforms can achieve similar performance as the ideal bi-orthogonal robust waveforms in high mobility scenarios.**

I. Introduction

Orthogonal time frequency space (OTFS) is a promising modulation scheme that can provide reliable and efficient wireless communications in high mobility scenarios [1]. High mobility incurs large Doppler spread, which might cause severe inter-carrier interference (ICI) in conventional multi-carrier modulation schemes such as orthogonal frequency division multiplexing (OFDM). On the other hand, the large Doppler spread can also be used to benefit system performance by means of Doppler diversity [2].

Waveform design plays an essential role in OTFS. It is shown in [1] that with transmitter and receiver pulses satisfying the time-frequency bi-orthogonal robust property, OTFS significantly outperforms OFDM. The ideal time-frequency bi-orthogonal robust waveforms support the simplest decoding scheme [1] and have been believed as the lower bound on the error performance of OTFS [3]. However, such pulses are practically unrealizable [1], [4]. Instead, the performance of OFDM-based OTFS systems with rectangular waveforms is evaluated in [3]. It is recently shown in [5] that the employment of practical bandlimited filter at the receiver can severely degrade the performance of OTFS with rectangular waveforms.

*A. Zhou and J. Wu are with the Department of Electrical Engineering, University of Arkansas, Fayetteville, AR 72701. †Y. Pan is with the Department of Computer Science and Computer Engineering, University of Arkansas, Fayetteville, AR 72701. ‡H. Lin is with the Department of Electrical and Electronic Systems Engineering, Osaka Metropolitan University, Osaka, Japan. ⋆J. Yuan is with the School of Electrical Engineering and Telecommunications, University of New South Wales, Australia.

Most existing studies on OTFS follow an OFDM-based implementation [6], where the continuous-time Wigner transforms are approximated by using discrete Fourier transform (DFT). The OFDM-based structure can reduce implementation complexity. However, it cannot accurately represent the impacts of continuous-time pulse shaping, which is important for OTFS system designs. Other than sampling and approximation of the continuous waveform, such systems also require the approximation of the physical channel, where the arbitrary delay or Doppler spread of the physical channel must be normalized or approximated to an integer multiple of the minimum delay domain interval and minimum Doppler domain spacing.

In this paper, we study the impacts of continuous-time pulse-shaping waveforms in OTFS systems with a matched filter based analog receiver. The study is performed in a precise manner by strictly following the Heisenberg and Wigner transforms as in the original OTFS architecture. Such an approach differs from the commonly used OFDM-based implementation that requires sampling and approximation of the continuous-time waveform. The impacts of the continuous-time waveforms are analytically quantified by developing closed-form expressions of cross-ambiguity functions of several practical pulses. With the help of the analytical cross-ambiguity functions, we develop a new matrix representation of the input-output relationship of the OTFS system by using an equivalent discrete delay-Doppler channel spread function that incorporates the combined effects of the physical propagation channel, the continuous-time pulse shaping waveforms, and the bandwidth and duration restrictions imposed on the OTFS signals. Simulation results show that under the analog OTFS architecture, practical rectangular pulse-shaping waveforms can achieve similar performance as ideal bi-orthogonal robust waveforms in high mobility scenarios.

II. System Model

A. OTFS Frame Structure

In the time-frequency domain, each OTFS frame contains N time symbols with symbol interval T and M subcarriers with subcarrier spacing Δf, where $\Delta f = \frac{1}{T}$. Consequently, the time interval between two consecutive OTFS frames in the time domain is NT, and the frequency spacing between two adjacent OTFS frames in the frequency domain is $M\Delta f$. It should be noted that the actual time duration (or bandwidth) of an OTFS frame might be larger than NT (or $M\Delta f$) based on the pulse-shaping waveform used during OTFS modulation.

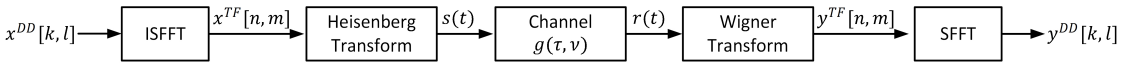

Fig. 1: The block diagram of an OTFS system.

The resolutions in the delay and Doppler domains are determined by the time duration and frequency range of the OTFS frame in the time-frequency domain. The minimum delay domain interval, $\Delta\tau$, and minimum Doppler domain spacing, $\Delta\nu$, are inversely proportional to, respectively, the frequency domain frame spacing, $M\Delta f$, and time domain frame interval, NT, as $\Delta\tau = \frac{1}{M\Delta f}$ and $\Delta\nu = \frac{1}{NT}$.

The delay-Doppler domain is discretized into an $N \times M$ grid with N levels in the delay domain and M levels in the Doppler domain. The delay span and Doppler spread of one OTFS frame is thus $M\Delta\tau = \frac{1}{\Delta f}$ and $N\Delta\nu = \frac{1}{T}$, respectively. $N \times M$ information symbols are modulated onto the delay-Doppler grid. Denote $x^{\text{DD}}[k,l]$ as the information symbol that is transmitted at delay $k\Delta\tau$ and Doppler shift $l\Delta\nu$, for $k = 0, \cdots, N-1$ and $l = 0, \cdots, M-1$.

B. OTFS System Architecture

The block diagram of an OTFS system is shown in Fig. 1. The delay-Doppler domain symbols are converted to the time domain by using the inverse symplectic finite Fourier transform (ISFFT) as

$$x^{\text{TF}}[n,m] = \frac{1}{\sqrt{NM}} \sum_{k=0}^{N-1} \sum_{l=0}^{M-1} x^{\text{DD}}[k,l] e^{j2\pi\left(\frac{nk}{N} - \frac{ml}{M}\right)}, \quad (1)$$

where $x^{\text{TF}}[n,m]$ is the time-frequency sample to be transmitted at time nT and subcarrier $m\Delta f$.

The time-frequency sample $x^{\text{TF}}[n,m]$ is then converted to the continuous time waveform $s(t)$ by means of multi-carrier modulation with a transmit pulse-shaping waveform $p_{\text{TX}}(t)$ as

$$s(t) = \sum_{n=0}^{N-1} \sum_{m=0}^{M-1} x^{\text{TF}}[n,m] p_{\text{TX}}(t-nT) e^{j2\pi m\Delta f(t-nT)}. \quad (2)$$

The above operation is also referred to as the (discrete) Heisenberg transform that is parameterized by $p_{\text{TX}}(t)$.

The continuous-time signal is transmitted through a time-varying channel. It is assumed that the channel impulse response (CIR) is decided by a small number of reflectors. Hence, only a few parameters are needed to model the channel in the delay–Doppler domain as

$$g(\tau,\nu) = \sum_{i=1}^{P} g_i \delta(\tau - \tau_i)\delta(\nu - \nu_i), \quad (3)$$

where $\delta(\cdot)$ is the Dirac delta function, g_i, τ_i, and ν_i are the path gain, delay, and Doppler shift for the i-th path, respectively, and P is the number of propagation paths.

It is worth noting that: 1) $g(\tau,\nu)$ captures the *physical* channel response that is only associated with the channel environment; 2) the delay τ_i and Doppler shift ν_i for path i can take *arbitrary* values that are determined by the physical propagation environment.

After passing through the time-varying channel, the signal observed at the receiver is

$$r(t) = \sum_{i=1}^{P} g_i s(t-\tau_i) e^{j2\pi\nu_i(t-\tau_i)} + z(t), \quad (4)$$

where $z(t)$ is additive white Gaussian noise (AWGN) with one-sided power spectral density N_0.

The received signal passes through a receiving filter $p_{\text{RX}}(t)$. The received signal is then converted to the time-frequency domain via the Wigner transform as

$$y(t,f) = \int p^*_{\text{RX}}(t'-t) r(t') e^{-j2\pi f(t'-t)} dt'. \quad (5)$$

The discrete time-frequency domain output of the matched filter is obtained by sampling $y(t,f)$ as

$$y^{\text{TF}}[n,m] = y(t,f)|_{t=nT, f=m\Delta f}, \quad (6)$$

where $n = 0, \ldots, N-1$ and $m = 0, \ldots, M-1$. Combining (2), (4), and (5), we have the time-frequency domain system equation as

$$y^{\text{TF}}[n,m] = \sum_{n'=0}^{N-1} \sum_{m'=0}^{M-1} h_{n,m}[n',m'] x^{\text{TF}}[n',m'] + z^{\text{TF}}[n,m], \quad (7)$$

where

$$z^{\text{TF}}[n,m] = \int_{-\infty}^{+\infty} p^*_{\text{RX}}(t'-nT) z(t') e^{-j2\pi m\Delta f(t'-nT)}\, dt' \quad (8)$$

is the noise sample in the time-frequency domain, and

$$\begin{aligned} &h_{n,m}[n',m'] \\ &= \sum_{i=1}^{P} g_i \cdot A_{p_{\text{RX}},p_{\text{TX}}}((n-n')T - \tau_i, (m-m')\Delta f - \nu_i) \\ &\quad \times e^{j2\pi(\nu_i + m'\Delta f)((n-n')T - \tau_i)} e^{j2\pi\nu_i n'T} \end{aligned} \quad (9)$$

is the equivalent discrete time-frequency spread function, with $A_{p_{\text{RX}},p_{\text{TX}}}(t,f)$ being the cross-ambiguity function between the two filters defined as

$$A_{p_{\text{RX}},p_{\text{TX}}}(t,f) = \int_{-\infty}^{\infty} p^*_{\text{RX}}(t'-t) p_{\text{TX}}(t') e^{-j2\pi f(t'-t)} dt'. \quad (10)$$

The time-frequency domain received samples can then be converted to the delay-Doppler domain by SFFT as

$$y^{\text{DD}}[k,l] = \frac{1}{\sqrt{NM}} \sum_{n=0}^{N-1} \sum_{m=0}^{M-1} y^{\text{TF}}[n,m] e^{-j2\pi\left(\frac{nk}{N} - \frac{ml}{M}\right)}, \quad (11)$$

for $k, l = 0, \cdots, N-1$.

We have the following comments regarding the time-frequency system equation given in (7).

Comment 1. The *equivalent* discrete time-frequency spread function, $h_{n,m}[n',m']$, incorporates the effects of the physical propagation channel, the pulse-shaping waveform, and the

bandwidth and duration restrictions imposed on the OTFS signals. The taps of the equivalent discrete time-frequency spread function are spaced by T seconds in the time domain and Δf Hz in the frequency domain, even though the physical propagation channel might have arbitrary delays and Doppler spreads. With the equivalent discrete time-frequency spread function given in (9), there is no need to normalize or approximate the arbitrary delay or Doppler spread of the physical channel to an integer multiple of $\frac{1}{M\Delta f}$ or $\frac{1}{NT}$.

Comment 2. In most commonly used OTFS implementations, the time-frequency domain samples $y^{\text{TF}}[n,m]$ are obtained by using DFT to represent the combined effects of the continuous-time Wigner transform in (5) and the subsequent sampling in (6). This leads to the low complexity OFDM-based implementation. However, based on the Nyquist sampling theorem, the OFDM-based implementation is precise only when the bandwidth of the OTFS waveform is less than $\frac{M}{2T}$. Otherwise, such an implementation is just an approximation of the original OTFS architecture. The analog receiver used in this paper, on the other hand, can precisely represent the behaviors of the analog Wigner transform by using cross-ambiguity functions.

III. Matrix Representation of Delay-Doppler Domain System Equation

In this section, we develop the delay-Doppler domain input-output relationship of the OTFS system in the matrix format.

A. Delay-Doppler Domain System Equation

The time-frequency system equation in (7) can be alternatively expressed in a matrix format as

$$\text{vec}\left(\mathbf{Y}^{\text{TF}}\right) = \mathbf{H}^{\text{TF}} \cdot \text{vec}\left(\mathbf{X}^{\text{TF}}\right) + \text{vec}\left(\mathbf{Z}^{\text{TF}}\right), \tag{12}$$

where the vector operator $\text{vec}\left(\mathbf{A}\right)$ returns a column vector by stacking the columns of the matrix $\mathbf{A}$, $\mathbf{Y}^{\text{TF}}$, $\mathbf{X}^{\text{TF}}$, $\mathbf{Z}^{\text{TF}}$ are $N\times M$ matrices with the (n,m)-th element being $y^{\text{TF}}[n,m]$, $x^{\text{TF}}[n,m]$, and $z^{\text{TF}}[n,m]$, respectively, and $\mathbf{H}^{\text{TF}}$ is a size $NM\times NM$ matrix, with the element on the $(mN+n)$-th row and $(m'N+n')$-th column being $h_{n,m}(n',m')$.

The conversion between time-frequency domain and delay-Doppler domain samples is achieved by means of ISFFT and SFFT. The ISFFT in (1) can be written in matrix format as

$$\mathbf{X}^{\text{TF}} = \mathbf{F}_N^H \cdot \mathbf{X}^{\text{DD}} \cdot \mathbf{F}_M, \tag{13}$$

where $\mathbf{F}_N$ is a size $N\times N$ discrete Fourier transform (DFT) matrix with the (k,l)-th element being $\frac{1}{\sqrt{N}}e^{-j\frac{2\pi kl}{N}}$, for $k,l=0,\cdots,N-1$, and $\mathbf{X}^{\text{DD}}$ is an $N\times M$ matrix with $x^{\text{DD}}[k,l]$ on the k-th row and l-th column.

The SFFT in (11) can be written in a matrix format as

$$\mathbf{Y}^{\text{DD}} = \mathbf{F}_N \cdot \mathbf{Y}^{\text{TF}} \cdot \mathbf{F}_M^H, \text{ or } \quad \mathbf{Y}^{\text{TF}} = \mathbf{F}_N^H \cdot \mathbf{Y}^{\text{DD}} \cdot \mathbf{F}_M. \tag{14}$$

With (13) and (14), we can rewrite the system equation in (12) as

$$\begin{aligned}\text{vec}\left(\mathbf{F}_N^H\mathbf{Y}^{\text{DD}}\mathbf{F}_M\right) =& \mathbf{H}^{\text{TF}} \cdot \text{vec}\left(\mathbf{F}_N^H\mathbf{X}^{\text{DD}}\mathbf{F}_M\right) + \\ & \text{vec}\left(\mathbf{F}_N^H\mathbf{Z}^{\text{DD}}\mathbf{F}_M\right),\end{aligned} \tag{15}$$

where $\mathbf{Z}^{\text{DD}} = \mathbf{F}_N \cdot \mathbf{Z}^{\text{TF}} \cdot \mathbf{F}_M^H$ is the delay-Doppler domain noise matrix.

With the identity $\text{vec}\left(\mathbf{AXB}\right) = \left(\mathbf{B}^T \otimes \mathbf{A}\right) \cdot \text{vec}\left(\mathbf{X}\right)$ [7, eqn. (520)], where $\otimes$ represents matrix Kronecker product, the delay-Doppler domain system equation of the OTFS system can be written in a matrix format as

$$\text{vec}\left(\mathbf{Y}^{\text{DD}}\right) = \mathbf{H}^{\text{DD}} \cdot \text{vec}\left(\mathbf{X}^{\text{DD}}\right) + \text{vec}\left(\mathbf{Z}^{\text{DD}}\right), \tag{16}$$

where $\mathbf{H}^{\text{DD}} \in \mathcal{C}^{NM\times NM}$ is the equivalent delay-Doppler domain channel matrix. It can be calculated by using the time-frequency domain channel matrix as

$$\mathbf{H}^{\text{DD}} = \mathcal{F}^H \cdot \mathbf{H}^{\text{TF}} \cdot \mathcal{F}, \tag{17}$$

where $\mathcal{F} = \mathbf{F}_M \otimes \mathbf{F}_N^H$ is an orthonormal matrix.

The matrix system equation in (16) describes the input-output relationship of an OTFS system with generalized pulse shaping waveforms $p_{\text{TX}}(t)$ and $p_{\text{RX}}(t)$. In the matrix system representation, the OTFS system is equivalently represented as a multiple-input multiple-output (MIMO) system with NM inputs and NM outputs.

The performance of the OTFS system (or the equivalent MIMO system) is determined by the statistical properties of the equivalent discrete delay-Doppler channel matrix $\mathbf{H}^{\text{DD}}$ and noise vector $\text{vec}\left(\mathbf{Z}^{\text{DD}}\right)$. The discrete delay-Doppler channel matrix $\mathbf{H}^{\text{DD}}$ incorporates the effects of the cross-ambiguity function of the pulse-shaping waveforms $p_{\text{TX}}(t)$ and $p_{\text{RX}}(t)$, the physical channel $g(\tau,\nu)$, and the sampling intervals in time-frequency and delay-Doppler domains.

B. Statistical Properties of Noise Samples

Due to the effects of the receiving pulse $p_{\text{RX}}(t)$, the noise samples in the delay-Doppler domain might be correlated. We have the following Lemma regarding the statistical properties of the delay-Doppler domain noise samples.

Lemma III.1. *The delay-Doppler domain noise sample vector, $vec\left(\mathbf{Z}^{DD}\right)$, is zero-mean complex Gaussian distributed with the covariance matrix being*

$$\mathbf{R}_{\mathbf{z}}^{DD} \triangleq \mathbb{E}\left[vec\left(\mathbf{Z}^{DD}\right) vec\left(\mathbf{Z}^{DD}\right)^H\right] = \mathcal{F}^H \cdot \mathbf{R}_{\mathbf{z}}^{TF} \cdot \mathcal{F}, \tag{18}$$

where $\mathbf{R}_{\mathbf{z}}^{TF}$ is the covariance matrix of the time-frequency domain noise vector as

$$\mathbf{R}_{\mathbf{z}}^{TF} \triangleq \mathbb{E}\left[vec\left(\mathbf{Z}^{TF}\right) vec\left(\mathbf{Z}^{TF}\right)^H\right] \in \mathcal{R}^{NM\times NM}. \tag{19}$$

The element on the (m_1N+n_1+1)-th row and the (m_2N+n_2+1)-th column of $\mathbf{R}_{\mathbf{z}}^{TF}$ is

$$\begin{aligned}\rho(m_1,n_1;m_2,n_2) = & N_0 \cdot e^{j2\pi m_2(n_1-n_2)\Delta fT} \\ & \times A_{p_{RX}p_{RX}}\left((n_1-n_2)T,(m_1-m_2)\Delta f\right),\end{aligned} \tag{20}$$

where $A_{p_{RX}p_{RX}}(t,f)$ is the cross-ambiguity function of the receiving pulse with itself. ■

All proofs in this paper are omitted due to space limit.

The values of the elements in the noise covariance matrix depend directly on the cross-ambiguity function of the receiving

filter, which usually assumes the same form as the pulse-shaping waveform at the transmitter, that is, $p_{\text{TX}}(t) = p_{\text{RX}}(t)$. We will study the behaviors of OTFS systems under various practical pulse-shaping waveforms and compare their performances to those with ideal pulse-shaping waveforms.

C. Receiver Design

With the system equation given in (16), the optimum maximum likelihood (ML) receiver can be designed as

$$\widehat{\mathbf{x}^{\text{DD}}} = \underset{\mathbf{x}^{\text{DD}} \in \mathcal{M}^{NM\times 1}}{\arg\min} \left[(\mathbf{y}^{\text{DD}} - \mathbf{H}^{\text{DD}}\mathbf{x}^{\text{DD}})^H (\mathbf{R}_{\mathbf{z}}^{\text{DD}})^{\dagger} (\mathbf{y}^{\text{DD}} - \mathbf{H}^{\text{DD}}\mathbf{x}^{\text{DD}})\right], \tag{21}$$

where $\mathbf{y}^{\text{DD}} = \text{vec}\,(\mathbf{Y}^{\text{DD}})$, $\mathbf{x}^{\text{DD}} = \text{vec}\,(\mathbf{X}^{\text{DD}})$, $\mathcal{M}$ is the set of modulation symbols, and $\mathbf{A}^{\dagger}$ represents matrix pseudo-inverse.

The complexity of the ML receiver grows exponentially with the modulation level and the size of N and M, and it becomes prohibitively high for larger values of N and M.

Suboptimum detection algorithms, such as message passing (MP) [3] or block decision feedback equalization (BDFE) [8], can be used to coherently combine the symbols in the delay-Doppler domain to achieve delay and Doppler diversity, while simultaneously suppress interference in both domains. It should be noted that for systems with colored noise, we need to first apply noise whitening filters to the received samples before applying the MP or BDFE algorithms.

In this paper, the detection is performed by using the optimum ML detector for small values of N and M, and BDFE for systems with larger N and M.

IV. Cross-Ambiguity Functions of Pulse-Shaping Waveforms

The cross-ambiguity functions of the pulse-shaping waveform play a critical role in the performance of OTFS systems. They affect the statistical properties of both the equivalent channel matrix and the noise samples in the delay-Doppler domain. We will develop the closed-form expressions of the cross-ambiguity functions of various pulse-shaping waveforms, and study their impacts on the performance of OTFS systems.

A. Ideal Time-Frequency Bi-orthogonal Waveform

A pair of pulse-shaping waveforms, $p_{\text{TX}}(t)$ and $p_{\text{RX}}(t)$, are said to satisfy the time-frequency bi-orthogonal robust property if their cross-ambiguity function satisfies [3]

$$A_{p_{\text{RX}},p_{\text{TX}}}(nT - \tau, m\Delta f - \nu) = \delta(n)\delta(m), \tag{22}$$

for any $\tau \in (-\tau_{\max}, \tau_{\max})$ and $\nu \in (-\nu_{\max}, \nu_{\max})$. It should be noted that the ideal bi-orthogonal pulse does not exist in practice due to the uncertainty principle.

Substituting (22) into (9) yields

$$h_{n,m}[n', m'] = \sum_{i=1}^{P} g_i \cdot \delta(n - n')\delta(m - m') \times e^{-j2\pi(m\Delta f + \nu_i)\tau_i} e^{j2\pi\nu_i nT}. \tag{23}$$

Thus, the CIR matrix $\mathbf{H}^{\text{TF}}$ reduces to a diagonal matrix, with the $(mN + n + 1)$-th diagonal element being

$$h_{n,m}[n, m] = \sum_{i=1}^{P} g_i e^{-j2\pi(m\Delta f + \nu_i)\tau_i} e^{j2\pi\nu_i nT}. \tag{24}$$

If we further assume that $p_{\text{RX}}(t)$ is bi-orthogonal with itself, then we have the following corollary regarding the statistical properties of the noise samples.

Corollary IV.1. *For an OTFS system with the ideal time-frequency bi-orthogonal waveforms, the noise samples in both the time-frequency and delay-Doppler domains are zero-mean white Gaussian random processes with variance N_0.* ■

It has been believed in the literature that the error performance of OTFS with the ideal time-frequency bi-orthogonal waveforms serves as a lower bound on the performance of OTFS systems [3], and it enables the simplest decoding [1].

However, it should be noted that even though the bi-orthogonal orthogonal pulses lead to a diagonal equivalent CIR matrix $\mathbf{H}^{\text{TF}}$ in the time-frequency domain, there will still be interference in the delay-Doppler domain as $\mathbf{H}^{\text{DD}} = \mathcal{F}^H \cdot \mathbf{H}^{\text{TF}} \cdot \mathcal{F}$. There is no theoretical justification that such time-frequency bi-orthogonal waveforms can lead to a performance lower bound in the delay-Doppler domain. We will show in this paper that the error performance of ideal waveforms does not necessarily serve as a lower bound for OTFS systems.

B. Rectangular Waveform

A rectangular pulse of duration T can be expressed as

$$p_{\text{RECT}}(t) = \begin{cases} \frac{1}{\sqrt{T}}, & 0 \le t \le T, \\ 0, & \text{otherwise.} \end{cases} \tag{25}$$

The cross-ambiguity function of $p_{\text{TX}}(t) = p_{\text{RX}}(t) = p_{\text{RECT}}(t)$ is given in the following proposition.

Proposition IV.1. *The cross-ambiguity function for rectangular waveforms with a duration T seconds is*

$$A_{RECT}(t, f) = \begin{cases} \frac{e^{j2\pi ft} - e^{-j2\pi fT}}{j2\pi fT}, & -T \le t \le 0, \\ \frac{1 - e^{j2\pi f(t-T)}}{j2\pi fT}, & 0 \le t \le T, \\ 0, & \textit{otherwise}. \end{cases} \tag{26}$$

■

The amplitude $|A_{\text{RECT}}(t, f)|$ is plotted as a function of the time variable t under various values of f in Fig. 2(a), where $T = \frac{1}{15\times 10^3}$ seconds. The cross-ambiguity function has final support in the time domain between $[-T, T]$, and its amplitude decreases monotonically as $|f|$ increases for a given t.

Corollary IV.2. *For an OTFS system with the length T rectangular pulse-shaping waveforms, the noise samples in both the time-frequency and delay-Doppler domains are zero-mean white Gaussian random processes with variance N_0.* ■

C. Sinc Waveform

A normalized sinc waveform with parameter T can be expressed as

$$p_{\text{SINC}}(t) = \frac{1}{\sqrt{T}} \cdot \text{sinc}\left(\frac{t}{T}\right). \tag{27}$$

The sinc waveform is the opposite of the rectangular waveform. It has unlimited time domain support but a rectangular spectrum in the frequency domain. Even though the sinc waveform has unlimited time domain support, it can be approximated by bounding the waveform over a finite time period, $[-KT, KT]$ given that its amplitude approaches 0 as $|t|$ becomes large.

The close-form expressions of the cross-ambiguity function of two sinc waveforms with parameter T is presented as follows.

Proposition IV.2. *For sinc waveforms with parameter T, the cross-ambiguity function is*

$$A_{\text{SINC}}(t,f) = \begin{cases} \frac{T}{\pi t}\sin\left(\frac{\pi t}{T} + \pi f t\right) e^{j\pi f t}, & -1/T \le f \le 0, \\ \frac{T}{\pi t}\sin\left(\frac{\pi t}{T} - \pi f t\right) e^{j\pi f t}, & 0 \le f \le 1/T, \\ 0, & \textit{otherwise}. \end{cases} \tag{28}$$

■

The amplitude $|A_{\text{SINC}}(t,f)|$ under various values of f is shown in Fig. 2(b). As expected, the cross-ambiguity function has unlimited time support, with the amplitude approaches zero as $|t|$ increases. On the other hand, it has finite frequency domain support between $|f| \le \Delta f = \frac{1}{T}$. Since Δf is the smallest interval in the frequency domain, there is interference only between two adjacent frequency domain samples.

Corollary IV.3. *For an OTFS system with the sinc waveform with parameter T, the noise samples in both the time-frequency and delay-Doppler domains are zero-mean white Gaussian random process with variance N_0.* ■

The sinc waveform can be considered as a special case of the raised cosine waveform with a roll-off factor $\beta = 0$. It should be noted that if we employ a raised cosine waveform with $\beta > 0$, there will be a correlation among noise samples, and noise correlation will impact the receiver design.

V. Simulation Results

The performances of OTFS systems with ideal time-frequency bi-orthogonal, rectangular, and sinc waveforms are studied and compared in this section. The carrier frequency is set at 4 GHz. The subcarrier spacing Δf is set at 15 KHz. The physical channel is generated with an EVA delay profile [9] under various speeds of the user equipment (UE).

Figure 3(a) shows the bit error rate (BER) performance of OTFS systems with ideal, rectangular, and sinc waveforms under different UE speeds, where the detection is performed

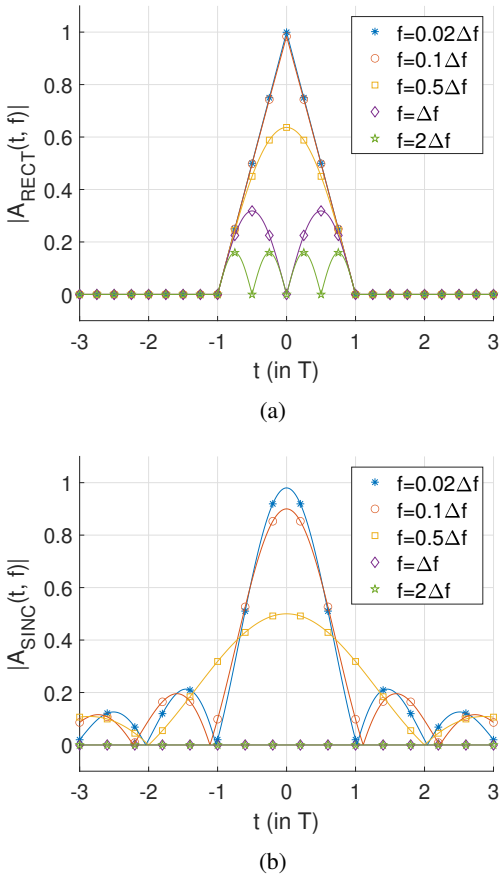

Fig. 2: Amplitude of cross-ambiguity function using (a) rectangular and (b) sinc pulses.

with the optimum ML detector to reveal the best possible performance of various waveforms. We set $N = 2$ and $M = 8$ with binary phase shift keying (BPSK) such that the ML detector can be employed with reasonable complexity. As expected, the BER performance improves with the increase of the UE speed due to the higher order of Doppler diversity. Under lower UE speeds, the performance of the various waveforms are very close to each other. At 30 km/hr, the ideal filter slightly outperforms the rectangular and sinc waveforms. At 100 km/hr, rectangular and ideal waveforms achieve almost identical performance. However, at 500 km/hr and BER = 10^{-3}, sysems with the rectangular or sinc waveforms slightly outperform their ideal filter counterpart by 0.63 and 0.42 dB, respectively. This can be explained by the fact that signals transmitted by the rectangular or sinc waveforms are more spread out in the delay-Doppler domain than those transmitted with the ideal waveform. As a result, the practical waveforms can achieve higher Doppler diversity order, but at the cost of more interference. The optimum ML detector can effectively harvest Doppler diversity while supressing interference. At high mobility scenario the effects of Doppler diversity dominate that of the interference, thus better performance is achieved by the practical waveforms.

Figure 3(b) shows the BER performance of OTFS systems with $N = 8$, $M = 32$ and quadrature phase shift keying

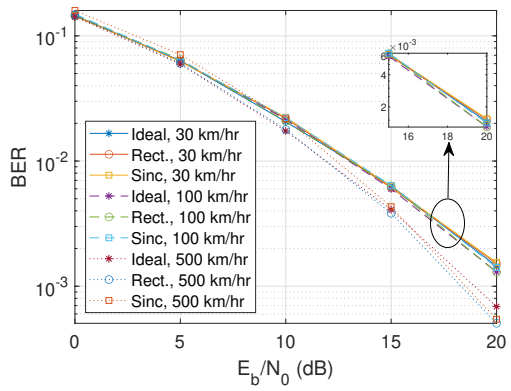

(a)

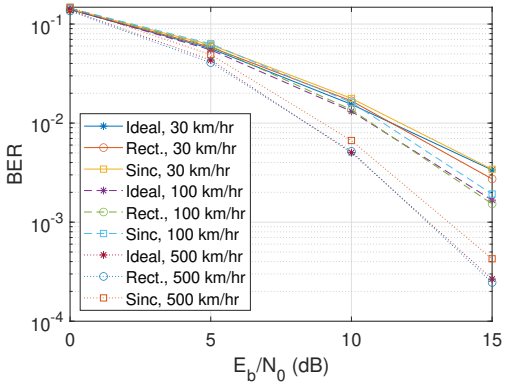

(b)

Fig. 3: The BER performance of OTFS with ideal, rectangular, and sinc pulses under different UE speeds, by using (a) optimum ML detector ($N = 2$, $M = 8$, BPSK), (b) BDFE detector ($N = 8$, $M = 32$, QPSK).

(QPSK) modulation, where the optimum ML detector can no longer be used due to the high complexity. The detection is performed by using the BDFE detector. Compared to the results in Fig. 3(a), systems with $N = 8$ and $M = 32$ achieve significant performance gains over those with $N = 2$ and $M = 8$. The performance gain is contributed by the higher Doppler and delay diversity orders due to larger values of N and M. The performance gains achieved at higher UE speeds are more prominent than the $N = 2$ and $M = 8$ case given the fact that more diversity gains can be achieved with larger N and M. At lower UE speeds (e.g. 30 or 100 km/hr), the performance of the three waveforms are very close to each other. At higher UE speed (e.g. 500 km/hr), the rectangular waveform and ideal bi-orthogonal robust waveform achieve almost identical performance, and both outperform the sinc waveform. Thus the BDFE detector can also effectively achieve the task of simultaneous coherent diversity combining and interference suppression.

It should be noted that the employment of rectangular (or sinc waveform) will lead to bandwidth (or time) extension of the OTFS signal in the time-frequency domain. In practical systems, we might need to pass the OTFS signal through a practical band-limiting filter, and this might cause distortion to the received OTFS signal and lead to error floors [5].

VI. Conclusions

We have studied the impacts of ideal and practical pulse-shaping waveforms on the performance of OTFS. The OTFS system was implemented by strictly following the structure of Heisenberg transform and Wigner transform with a matched filter based analog receiver. Such an approach is different from most commonly used OTFS implementation with a sampling and DFT-based digital receiver, which uses discretized waveforms to approximate the Wigner transforms with continuous-time waveforms. The employed analog receiver represents the impacts of continuous-time pulse-shaping waveforms in a precise manner, and it does not require the various approximations used by existing works. We have proposed a new matrix representation of the OTFS system, where the equivalent discrete delay-Doppler domain channel spread function captures the effects of *continuous-time* pulse shaping waveform, the physical propagation channel, and the bandwidth and duration restrictions imposed on the OTFS signals. It has been shown that the system performance depends critically on the cross-ambiguity functions of the pulse shaping waveforms. We have developed closed-form expressions of the cross-ambiguity functions of various practical waveforms. Simulation results show with the analog receiver, practical waveforms, such as the rectangular waveform, can achieve almost identical performance as the ideal non-realizable time-frequency bi-orthogonal robost waveforms under high mobility scenarios.

References

[1] R. Hadani, S. Rakib, M. Tsatsanis, A. Monk, A. J. Goldsmith, A. F. Molisch, and R. Calderbank, "Orthogonal time frequency space modulation," in *2017 IEEE Wireless Communications and Networking Conference (WCNC)*. IEEE, 2017, pp. 1–6.

[2] W. Zhou, J. Wu, and P. Fan, "High mobility wireless communications with doppler diversity: Fundamental performance limits," *IEEE Transactions on Wireless communications*, vol. 14, no. 12, pp. 6981–6992, 2015.

[3] P. Raviteja, K. T. Phan, Y. Hong, and E. Viterbo, "Interference cancellation and iterative detection for orthogonal time frequency space modulation," *IEEE transactions on wireless communications*, vol. 17, no. 10, pp. 6501–6515, 2018.

[4] P. Raviteja, Y. Hong, E. Viterbo, and E. Biglieri, "Practical pulse-shaping waveforms for reduced-cyclic-prefix OTFS," *IEEE Transactions on Vehicular Technology*, vol. 68, no. 1, pp. 957–961, 2018.

[5] C. Shen, J. Yuan, and H. Lin, "Error performance of rectangular pulse-shaped OTFS with practical receivers," *IEEE Wireless Communications Letters*, 2022.

[6] A. Farhang, A. RezazadehReyhani, L. E. Doyle, and B. Farhang-Boroujeny, "Low complexity modem structure for OFDM-based orthogonal time frequency space modulation," *IEEE Wireless Communications Letters*, vol. 7, no. 3, pp. 344–347, 2017.

[7] K. B. Petersen, M. S. Pedersen *et al.*, "The matrix cookbook," *Technical University of Denmark*, vol. 7, no. 15, p. 510, 2008.

[8] J. Wu and Y. R. Zheng, "Oversampled orthogonal frequency division multiplexing in doubly selective fading channels," *IEEE Transactions on Communications*, vol. 59, no. 3, pp. 815–822, 2010.

[9] ETSI LTE, "Evolved universal terrestrial radio access (E-UTRA); base station (BS) radio transmission and reception (3GPP TS 36.104 version 8.6. 0 release 8), july 2009," *ETSI TS*, vol. 136, no. 104, p. V8, 2009.